ADVANCED
SCIENCE NEWS
www.advancedsciencenews.com

NANO MICRO
small

Injectable Hydrogels

An Injectable Hybrid Hydrogel with Oriented Short Fibers Induces Unidirectional Growth of Functional Nerve Cells

Abdolrahman Omidinia-Anarkoli, Sarah Boesveld, Urandelger Tuvshindorj, Jonas C. Rose, Tamás Haraszti, and Laura De Laporte*

To regenerate soft aligned tissues in living organisms, low invasive biomaterials are required to create 3D microenvironments with a structural complexity to mimic the tissue's native architecture. Here, a tunable injectable hydrogel is reported, which allows precise engineering of the construct's anisotropy in situ. This material is defined as an Anisogel, representing a new type of tissue regenerative therapy. The Anisogel comprises a soft hydrogel, surrounding magneto-responsive, cell adhesive, short fibers, which orient in situ in the direction of a low external magnetic field, before complete gelation of the matrix. The magnetic field can be removed after gelation of the biocompatible gel precursor, which fixes the aligned fibers and preserves the anisotropic structure of the Anisogel. Fibroblasts and nerve cells grow and extend unidirectionally within the Anisogels, in comparison to hydrogels without fibers or with randomly oriented fibers. The neurons inside the Anisogel show spontaneous electrical activity with calcium signals propagating along the anisotropy axis of the material. The reported system is simple and elegant and the short magneto-responsive fibers can be produced with an effective high-throughput method, ideal for a minimal invasive route for aligned tissue therapy.

In many complex tissues (e.g., nerves and muscles), cells are surrounded by an extracellular matrix (ECM) with a specific anisotropic architecture.[1] These native 3D hierarchical structures influence the biological functions of tissues and allow for efficient cell–cell communication.[2] To successfully regenerate diseased or injured tissues with endogenous cells, biomaterial scaffolds have to support and instruct local cells to rebuild new healthy and functional tissue. Besides the mechanical and biochemical properties, the scaffold needs to

mimic the specific architectures of the ECM. Diverse techniques have been developed to engineer 3D implantable constructs, which are premade beforehand and exhibit highly ordered nano, micro, and macroscopic structures.[3] Methods to fabricate implantable scaffolds with unidirectional orientation entail magnetic alignment of proteins in the presence of a strong magnetic field (a few Teslas),[4] freeze-drying,[5] a gas foaming/particulate leaching method,[6,7] aligned fibers without or within hydrogels,[8] short-pulse lasers,[9] and using shear flow.[10] Especially in the case of nerve regeneration, polymeric anisotropic implants and aligned fibers have promoted directional nerve growth[11,12] and reduced scar formation at the lesion site after spinal cord injury (SCI).[13,14] Most aligned nanofibers are generated by electrospinning, which is a well-known and diverse approach with the ability to tailor the physical and biological properties of nanofibers.[11,15] The chemistry, surface wettability, degradation, mechanical properties, and surface topography can easily be manipulated by tuning the process parameters and applying various synthetic and/or natural materials.[16] However, one limitation of

A. Omidinia-Anarkoli, S. Boesveld, U. Tuvshindorj,
J. C. Rose, Dr. T. Haraszti, Dr. L. De Laporte
DWI Leibniz Institute for Interactive Materials
Aachen 52074, Germany
E-mail: delaporte@dwi.rwth-aachen.de

The ORCID identification number(s) for the author(s) of this article can be found under https://doi.org/10.1002/smll.201702207.

implantable materials is that a space has to be available or created by an invasive surgical procedure, which may lead to further impairment of the tissue.

To avoid causing additional damage to sensitive tissues, many applications, including therapies for spinal cord repair, require a minimal invasive material. In the case of acute SCI, it is crucial to spare all nerves that may still be intact or functional. Injectable materials, such as hydrogels, have the advantage that they can be injected as a liquid and form a matrix in situ.[17] This enables easy adaptation to irregular injury shapes and the creation of an integrative tissue-implant interface.[18] Hydrogels have been mixed with short fibers for cardiac regeneration[19] and hydrogel reinforcement.[20] Beyond different reported techniques, such as ultra-sonication,[21] homogenizing,[22] chemical treatment,[23] and patterned UV-crosslinking,[24] the electrospinning/microcutting method enables the production of quasi monodisperse short fibers,[25] which is crucial to control and study cell–fiber interactions.

Nevertheless, most injectable hydrogels consist of an isotropic network and do not combine the required compliance and biomolecular functionalization with orientational order.[17,18] Over the past years, only few developments have been reported to introduce anisotropy or unidirectional guidance inside low invasive materials, which can be grouped in the following three examples. First, the alignment of dia-magnetic proteins uses high magnetic fields (>4.5 T), but this approach has only been used to fill the lumen of implants and has not yet been applied after injection in vivo. Second, self-assembling peptide amphiphiles that are able to form flow-induced oriented high-aspect-ratio nanofibers after a heating/cooling treatment.[26] To orient this hydrogel inside the spinal cord aligned with the nerves, the material has to be injected parallel to the spinal cord tissue using a micromanipulator-assisted needle retraction, which is challenging in clinical applications and can cause further damage. In addition, the formed nanofiber bundles have a small diameter of 40 nm, which limits the control and flexibility over the anisotropic dimensions of the hydrogel.[27] As a third approach, multiple groups have aligned magnetic particles inside a hydrogel to form colloidal assemblies in the direction of low magnetic fields in the milli Tesla (mT) range.[28,29] Here, it is difficult to control the dimensions, distances, and properties of the guiding elements, and more importantly, the magnetic particle strings consist entirely of iron oxide particles. Therefore, this method is not ideal for clinical use due to the high concentrations of iron oxide above the toxicity level for nerve cell applications.[30] In one example, spherical ECM-coated magnetic particles (300 nm) were oriented in Matrigel but demonstrated directed cell growth both parallel and perpendicular to the direction of strings due to the presence of a microspaced fibril pattern and nanoscale grooves, respectively.[28] Another study illustrated that the magnetic colloidal assembly of the particles resulted in alignment of the collagen fibers in the surrounding hydrogel.[29]

Alternatively, to reduce the amount of required iron oxide, macroscopic anisotropic elements with controlled dimensions and properties can be rendered magnetic by coating their surface with superparamagnetic iron oxide nanoparticles (SPIONs), or mixing superparamagnetic cobalt nanoparticles inside their volume, resulting in alignment in external mT magnetic fields.[31] We recently applied this concept to create biocompatible anisotropic hydrogels in situ.[32] A mold-based soft lithography batch approach was applied to fabricate rod-shaped microgels loaded with a low dose of SPIONs that orient in mT magnetic fields, after which they are fixed in a crosslinked hydrogel. The resulting anisotropic hybrid hydrogel is called an Anisogel. Even though the poly (ethylene oxide) microgels are not cell adhesive, they are able to prompt the cell's and nerve's decision to grow unidirectionally with only a minimal amount of structural guidance cues. To enhance the applicability of this method in the clinic and address many anisotropic tissues in the body (e.g., nerve, muscles, and heart), we here describe a novel straightforward and high-throughput fabrication method to fabricate Anisogels.

In this report, we demonstrate the development of a simple but effective concept to fabricate short, magneto-responsive poly (lactide-co-glycolide) (PLGA) fibers with controlled and defined diameters and lengths using a high-throughput, semicontinuous electrospinning/microcutting method. The short fibers are mixed within a precursor solution to introduce aligned, cell adhesive guiding elements inside an injectable hydrogel. PLGA is applied, as it is a clinically used and degradable biomaterial that has demonstrated to support nerve growth.[7] After collecting aligned PLGA nanofibers using a parallel plate collector, the fibers are embedded and fixed in a cryomedium to enable microsectioning perpendicular to the direction of the fibers (**Figure 1**a, steps I and II, and Figure S2, Supporting Information). By mixing SPIONs inside the PLGA solution before electrospinning, magnetically responsive short fibers are obtained, which are then dispersed inside the hydrogel precursor solution (Figure 1a, step III). A low magnetic field ($\leq$ 300 mT) is applied to this mixture, inducing short fiber orientation before hydrogel crosslinking, which results in the formation of our Anisogel (Figure 1a, step IV). Due to simplicity and reliability of this technique, the features of the anisotropic matrix can be controlled in situ with precise engineering. Compared to previously published reports,[28,29] the Anisogel only requires a low amount of iron oxide magnetic nanoparticles to orient the microscopic fibers, which are made of a nonmagnetic, cell adhesive polymer, using a high-throughput fabrication method. While the minimal application of iron oxide particles and the use of clinically approved biomaterials render the presented Anisogel favorable for in vivo applications,[30,33] the straightforward and effective fabrication method makes this system an excellent candidate for clinical translation.

PLGA fibers are electrospun and collected in an aligned manner with a diameter of 689.7 $\pm$ 88.5 nm (Figure 1b). They are cut into short fibers with four different fiber lengths: 25.5 $\pm$ 1.8 µm, 51.1 $\pm$ 2.8 µm, 78.5 $\pm$ 1.2 µm, and 101.1 $\pm$ 5.0 µm (Figure 1c). The parallel plate collector enhances the evaporation rate of the solvent, avoiding fiber fusion and resulting in single filaments. To render the short fibers magnetic, SPIONs with an average diameter of 5.2 $\pm$ 1.0 nm (Figure S1a, Supporting Information) are synthesized
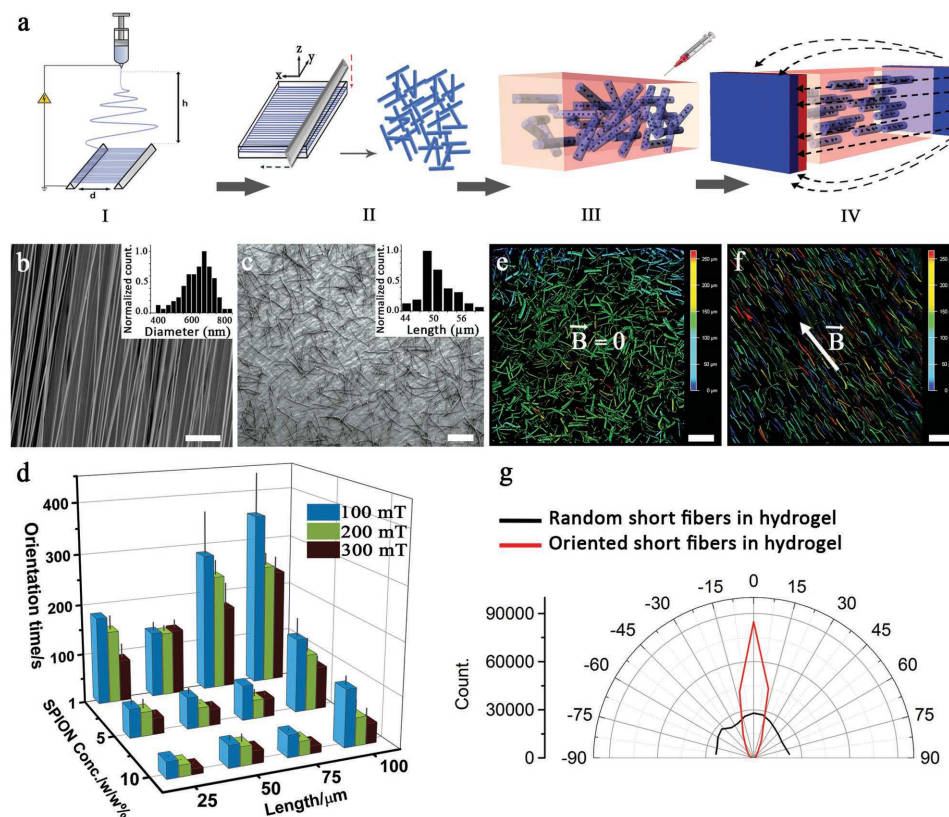
Figure 1. a) A schematic representation of the Anisogels fabrication process. Electrospinning of aligned fibers on a parallel plate (step I), followed by embedding the fibers in an optimum cutting temperature (OCT) gel for subsequent cryosectioning. The fibers are purified and dispersed in distilled water after melting and washing off the excess of gel (step II). Randomly oriented short fibers mixed within the hydrogel precursor solution in liquid state before applying the magnetic field (step III). Fiber orientation and hydrogel solidification result in the Anisogel (step IV). b) SEM image of aligned PLGA fibers formed on a parallel plate collector with an average diameter of 689.7 ± 88.5 nm (inset: diameter distribution histogram). c) SEM image of 50 µm short fibers after cryosectioning (inset: length distribution histogram). Scale bars 50 µm. d) The orientation time of magneto-responsive short fibers with different lengths and SPION concentrations at three different magnetic fields. Depth color-coded images of magnetic fibers inside 3D fibrin hydrogels, prepared e) in the absence of an external magnetic field and f) in the presence of a 100 mT magnetic field. Scale bars 100 µm. g) The angular distribution of random and oriented fibers in a 3D hydrogel corresponding to (e,f), respectively.

and dispersed at different concentrations of 1, 5, and 10 w/w% inside the polymer solution before the electrospinning process. The SPIONs are homogenously distributed inside the PLGA solution and do not show any aggregation in solution, even after 1 h, which is the time it takes to spin the fibers (Figure S1b,c, Supporting Information). This is further confirmed by the visualization of homogenously distributed SPIONs inside the PLGA fibers after electrospinning (Figure S1d, Supporting Information). The average diameter of the obtained fibers is not affected by the incorporation of the SPIONs (Figure S3a, Supporting Information). Thermogravimetric analysis of the SPIONs reveals a 31.0 ± 0.5 w/w% iron content in the dried SPIONs and 78% SPION encapsulation efficiency inside the fibers during the production of the short fibers (Figure S3b,c, Supporting Information). By applying a magnetic field in the mT range, the short magneto-responsive fibers align their principal axis of magnetization relative to the direction of the magnetic field lines, as shown in Movie S1 in the Supporting Information. The effect of fiber length, SPION content, and the strength of the external magnetic field on fiber orientation is shown in Figure 1d. The orientation time of the short fibers decreases with increasing SPION concentration and magnetic field strength, while

increasing fiber length slows down the orientation rate. A minimum orientation time of 11.7 ± 2.1 s is achieved for fibers with a length of 25 µm, containing 10 w/w% SPIONs, in a magnetic field of 300 mT. Fibers with a length of 100 µm and 1 w/w% SPIONs demonstrate the longest orientation time of 350.0 ± 84.9 s in a 100 mT magnetic field. Reducing the length from 100 to 25 µm leads to a reduction in orientation time between 40% and 70%, depending on the SPION content and magnetic field strength. Fibers, produced with a length larger than 150 µm, and thus an aspect ratio higher than 200, give rise to physical entanglement and lose their ability to align. As the PLGA polymer solution is subjected to a high electric field during the electrospinning process, the polymer chains within the electrospun fibers have a high degree of alignment and orientation.[34] This leads to the relaxation of extended amorphous chains to a random coil state near the glass transition temperature (Tg ≈ 38 °C), causing a dimensional change (≈40% shrinkage) of the fibers at 37 °C. Therefore, for further use inside the Anisogels, the fibers are cut at a length of 100 µm, and preshrunk to ≈60 µm. To investigate the ability of the Anisogels to direct cell and nerve growth, the oriented fibers are interlocked inside a crosslinked hydrogel. Fibrin was chosen as a biocompatible
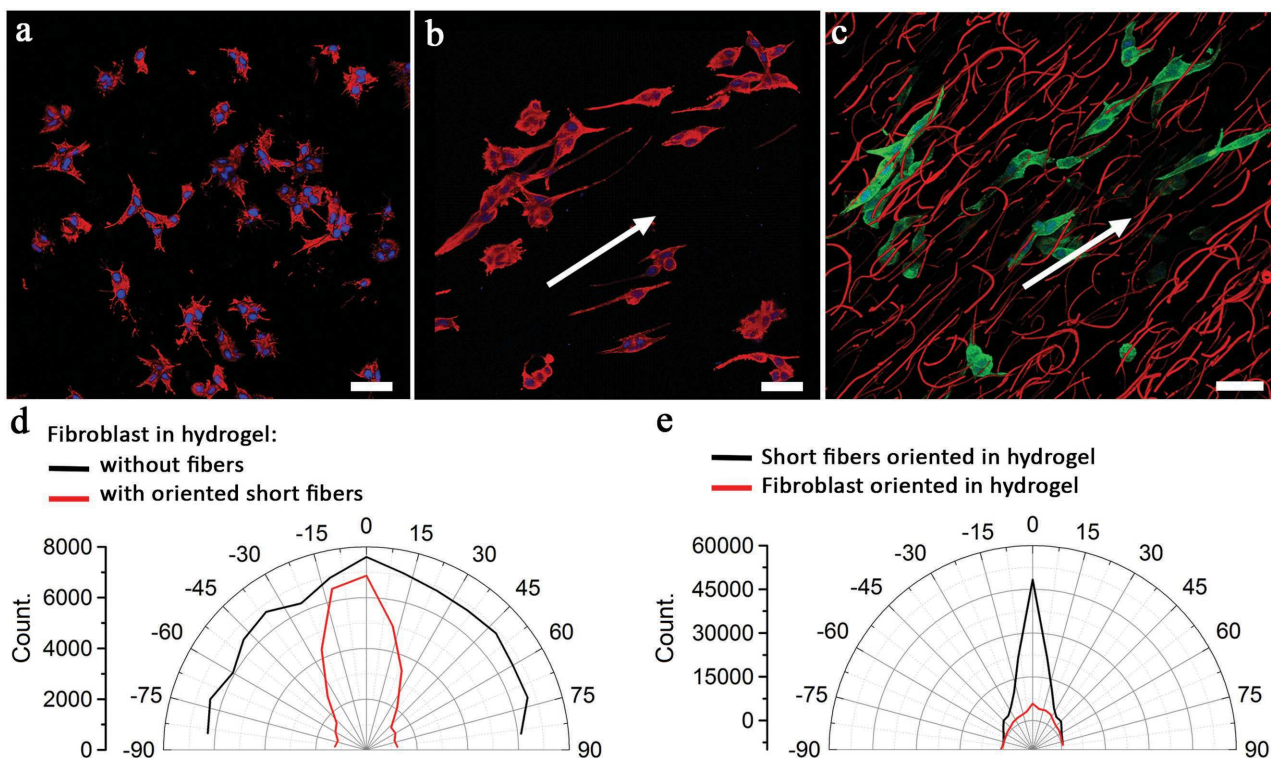
Figure 2. The ability of the Anisogel to direct cell growth. a) Fibroblasts mixed within a fibrin gel without fibers, F-actin filaments (red: Alexa Fluor 594 phalloidin) stretched in all directions. b) Fibroblasts mixed within a fibrin gel with short oriented fibers, F-actin filaments (red: Alexa Fluor 594 phalloidin) elongate in the direction of the aligned fibers (inset arrow). c) Fibroblasts (F-actin filaments stained in green: Alexa Fluor 488 phalloidin) elongate in the direction of the oriented fibers (red: Rhodamin B). Scale bars 50 µm. d) The angular distributions of fibroblast orientation in a 3D hydrogel without fibers and inside the Anisogel, corresponding to (a,b), respectively. e) The angular distribution of fibroblast and fiber orientation inside the Anisogel, corresponding to (c).

model hydrogel system to provide a microenvironment with the appropriate mechanical and biochemical properties for these cell cultures.[14] Magnetic fibers with a final approximate length of 60 µm are mixed within a fibrinogen solution with 0.25 U mL^{-1} Thrombin and 4 U mL^{-1} Factor XIII to tune the gelation kinetics of the gel and enable orientation and fixation of the fibers inside the 3D matrix. A fibrin composition with 4 mg mL^{-1} fibrinogen leads to a hydrogel storage modulus of 424.3 ± 94.0 Pa (Figure S4, Supporting Information), which is consistent with reported data and has demonstrated to support nerve growth.[35] In the absence of a magnetic field, randomly oriented fibers are obtained inside the fibrin gel (Figure 1e), which increases the storage modulus to 687.0 ± 28.8 Pa. This is in agreement with reported reinforced hydrogels, incorporated with randomly oriented short polymeric fibers.[36] In the presence of a low external magnetic field of 100 mT, the short fibers align unidirectionally, parallel to the field, while the fibrinogen solution crosslinks around the fibers, forming the Anisogel. This preserves the linear structure of the Anisogel after removal of the magnetic field (Figure 1f). The bulk storage modulus of these Anisogels is 572.7 ± 66.5 Pa, thus 16.6% lower compared to hydrogels with randomly oriented fibers, which is likely due to the less pronounced fiber entanglement with the hydrogel network, compared to randomly oriented fibers. Although this is an interesting observation, the main aim of this work is to provide linear guiding elements inside a soft hydrogel to direct

cells, changing the local mechanical properties. The magnetic alignment of the short fibers was successful as the full width half maximum (FWHM) of the angular distribution of the aligned fibers inside the hydrogel is 25.5°, compared to 171.0° in the absence of a magnetic field (Figure 1g and Figure S6a, Supporting Information).

The effect of the Anisogel on cell morphology and directional growth is evaluated by incorporating L929 mouse-derived fibroblasts, primary neurons, or full embryonic chick dorsal root ganglia (DRG) inside the gels. In the case of fibroblasts, a hydrogel without fibers, thus lacking unidirectional spatial guidance cues, induces multidirectional cell growth. Here, isotropic morphologies of the cells are observed with F-actin filaments stretched in all direction (**Figure 2**a). On the other hand, Anisogels containing only 0.015 v/v% short fibers lead to unidirectional cell growth along the fiber orientation with cells displaying an elongated shape and cytoskeleton (Figure 2b). Elongated fibroblasts are observed to adhere and grow along the oriented short fibers (Figure 2c). The angular distribution of fibroblast elongation inside the Anisogel shows a much narrower peak (FWHM: 54.4° ± 4.3°), compared to the hydrogel without fibers (FWHM: 162.5° ± 6.6°) (Figure 2d, Figure S6b, Supporting Information). The angular distributions of aligned fibroblasts and short fibers both show the same direction and have FWHMs of 49.0 ± 6.7 and 24.7 ± 11.8, respectively (Figure 2e).
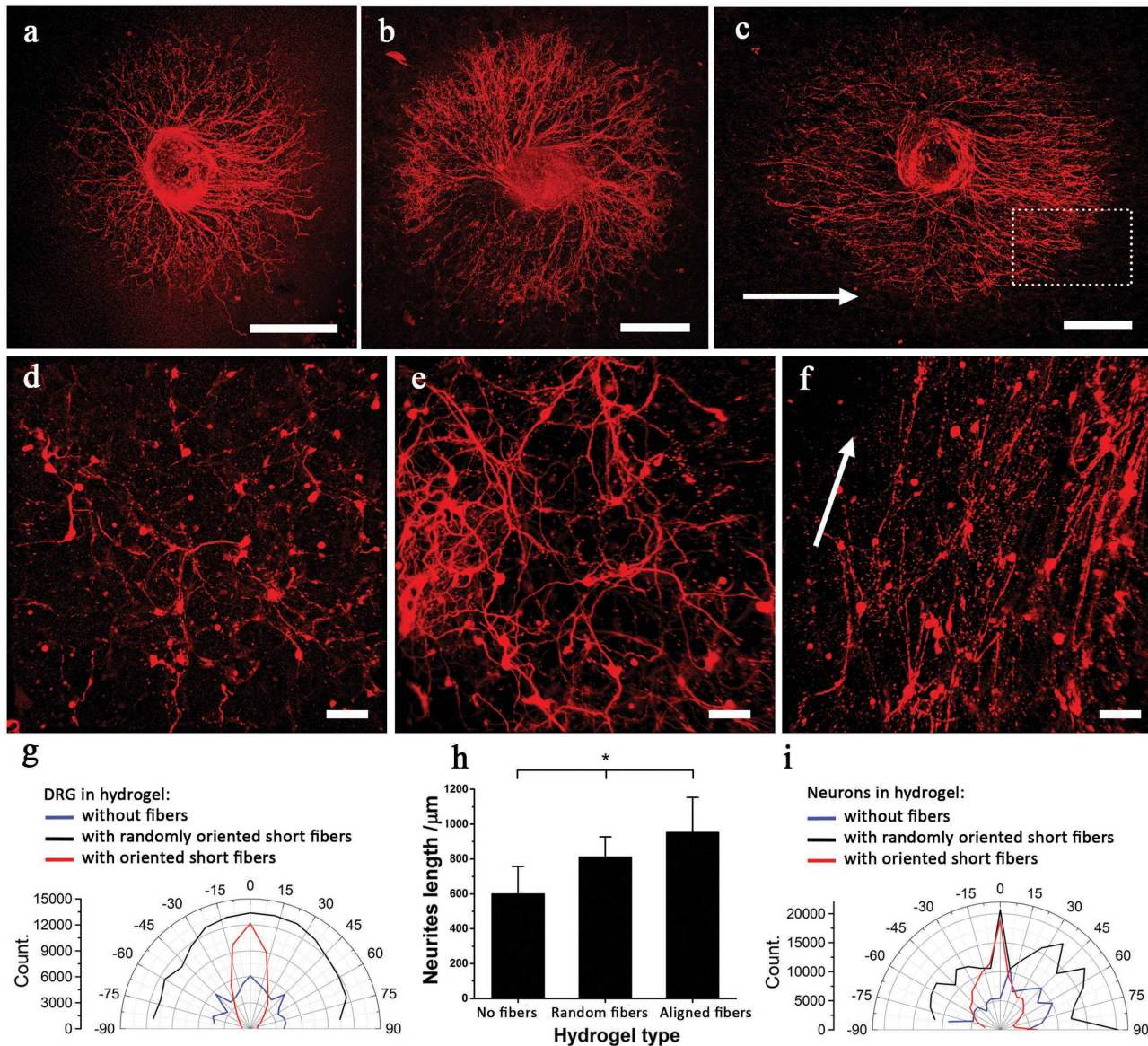
Figure 3. The ability of the Anisogel to support unidirectional nerve growth. DRG extension (red: ß tubulin detected with TRITC) in a hydrogel comprising a) no fibers, b) randomly oriented fibers, or c) unidirectionally oriented fibers (inset arrow). The white-dashed box in (c) is magnified in Figure S7a in the Supporting Information. Scale bars 500 µm. Neurite extensions of single neurons (red: ß tubulin detected with TRITC) in a hydrogel comprising d) no fibers, e) randomly oriented fibers, or f) unidirectionally oriented fibers (inset arrow). Scale bars 100 µm. g) The angular distributions of random and aligned DRG extensions in 3D hydrogels, corresponding to (a,b,c), respectively. h) Length of neurite extensions from a DRG explant in a hydrogel comprising either random or oriented short fibers, compared to a hydrogel without any fibers. i) The angular distribution of random and aligned neurite extensions of single neurons, corresponding to (d,e,f), respectively.

To analyze the potential of this Anisogel as a therapy for spinal cord repair, full DRG or dissociated primary neurons are, respectively, inserted or directly mixed into the hybrid hydrogels. The cells are cultured for 7 d to study in which direction neurites extend and migrate within the gels. Here, placing the DRG in both hydrogels without or with randomly oriented fibers results in radial extension of the growing neurites (**Figure 3**a,b), while the Anisogel triggers the neurites to grow along the fiber direction (Figure 3c and Figure S7a, Supporting Information). As shown in Figure 3g, the angular distribution of DRG neurite extensions in Anisogels demonstrates a narrower peak (FWHM: 59.6° ± 15.4°), compared to the gel in the absence of fibers (FWHM: 169.0° ± 2.8°) or

randomly oriented fibers (FWHM: 170.8° ± 0.3°) (Figure S6c, Supporting Information). Interestingly, despite the fact that both hydrogels with randomly oriented fibers and without any fibers result in radial nerve growth, hydrogels containing either aligned or random short fibers enhance the rate of neurite extension by 55% and 34%, respectively, compared to fibrin gels without any fibers (Figure 3h). This may be explained by the cell adhesive properties of PLGA.

In addition, experiments with single neurons confirm the functionality of in situ fiber alignment. Even though both hydrogels without fibers or with randomly oriented fibers show nerve extensions in all directions (Figure 3d,e, respectively), neurons mixed within Anisogels lead to elongation
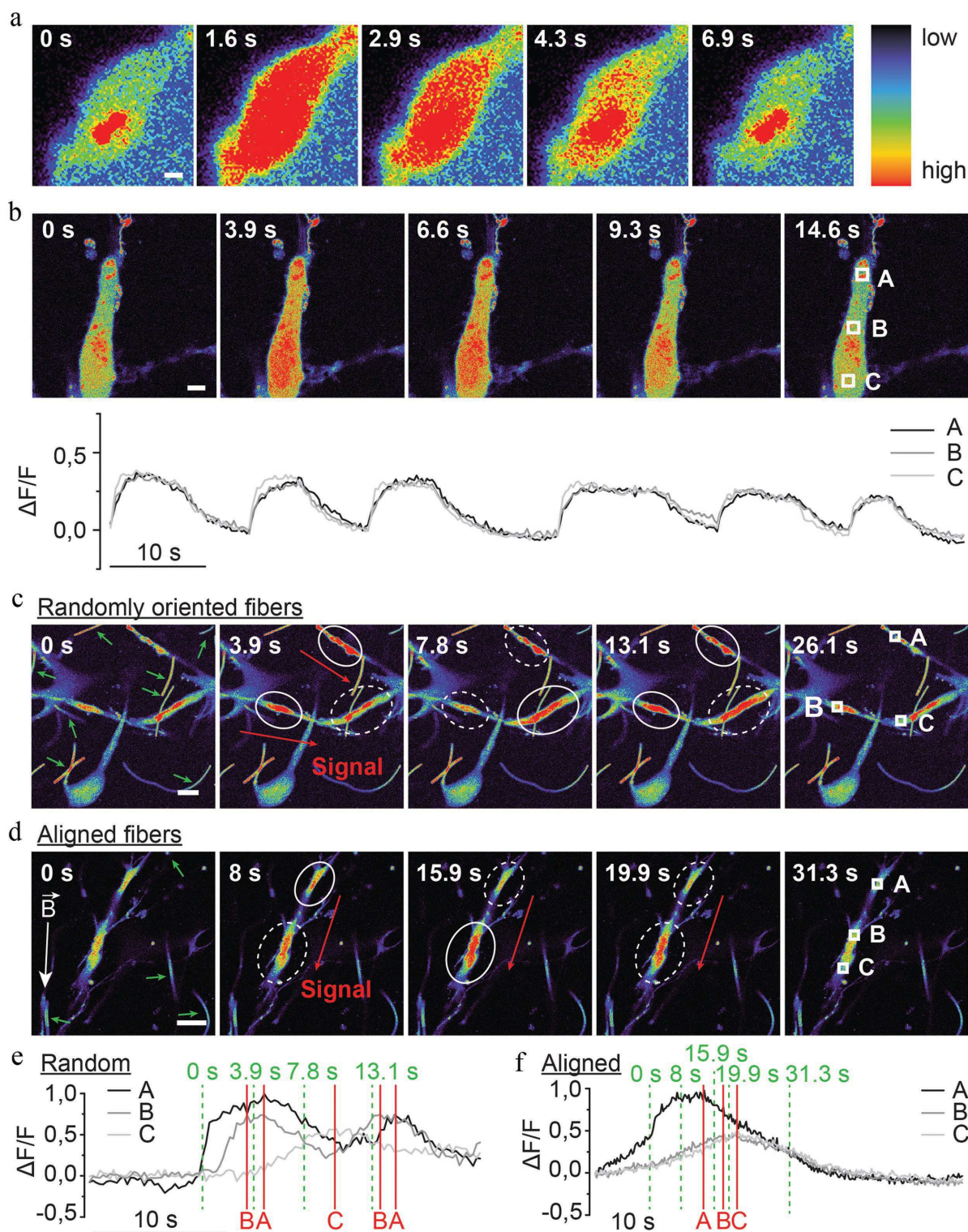
Figure 4. Neurons grown in an Anisogel are functional and demonstrate spontaneous electrochemical activity in the direction of the material and its anisotropy. a) Magnified image sequence of measured calcium signals of a neuronal cell inside an Anisogel corresponding to Movie S3 in the Supporting Information. b) Image sequence and quantification of a calcium transient in in three specific regions of interest (3 × 3 µm) inside a nerve cell in an Anisogel, corresponding to Movie S2 in the Supporting Information. Calcium peaks of similar size and frequency are observed over a course of 90–140 s. Effect of fiber orientation on the direction of neural signal propagation. Neurons are cultured inside fibrin hydrogels with c) randomly oriented fibers, or d) aligned fibers. The calcium signal direction is marked by the red arrows, while the green small arrows indicate fibers. A solid circle corresponds to a maintained or increasing signal, compared to the previous image, while a dashed circle corresponds to a fading signal. e–f) Normalized quantification (to mean ground signal F) of the calcium signals in (c,d), respectively, in three different regions of interest (3 × 3 µm) along the neurons (white boxes A, B, and C). Red lines show signal peak maxima and therefore the signal order and green lines indicate the time points of the images in c and d, respectively. Scale bar: a) 1 µm and c,d) 20 µm.

parallel to the aligned fibers (Figure 3f and Figure S7b, Supporting Information). The quantification of the angular distributions of the images confirms this trend, as the FWHM value for neurons mixed within a gel comprising aligned fibers (Figure 3f) is 33.2°, compared to 171.0° and 168.5° for gels without fibers (Figure 3d) or randomly oriented fibers (Figure 3e), respectively.

In order to investigate the functionality of the growing neurons inside the gels, we measure the calcium transient through a fluorescent indicator (Fluo-4). The nerve cells inside the Anisogel spontaneously and regularly excite, indicating electrochemically functional neuronal activity (**Figure 4**a, Movies S2–S4, Supporting Information). Quantification of the neuronal signals reveal peaks of similar size and frequency over a course of 90–140 s (Figure 4b, Figure S8, Movies S2–S4, Supporting Information). These signals are measured in 3D, and their parameters strongly depend on the local neuronal connectivity and therefore, neuronal density.[37] In addition, the effect of the material anisotropy on the neuronal activity is analyzed by measuring the calcium transient at lower magnifications. Quantification of the cellular calcium levels in different regions of interest (white boxes A, B, and C) is performed along the neuronal cells inside the hydrogels and substantiates the time lag between calcium transitions inside and along the different cells. Importantly, fibrin hydrogels with randomly oriented fibers show multidirectional signal propagation inside the gels (Figure 4c,e, Movie S5, Supporting Information), while aligned fibers induce signal propagation in the direction of the fibers, indicating Anisogel-directed neuronal activity (Figure 4d, Movie S6, Supporting Information). Signal frequency quantification shows a time lag between the different regions of interest (white boxes A, B, and C) along the aligned neurons, parallel to the direction of the fibers (Figure 4f). This Anisogel is the first injectable gel that demonstrates unidirectionally signal propagation along oriented nerves, which is an important and crucial function for further medical applications.

In conclusion, we demonstrate the potential of a novel, low invasive, anisotropic hydrogel, consisting of magneto-responsive, cell adhesive short fibers, and a crosslinked precursor solution. The micrometer-scale fibers are prepared by an effective high-throughput electrospinning/microcutting technique with tailorable dimensions. Encapsulation of low SPION doses during the spinning process leads to magneto-responsive behavior in the presence of an external magnetic field in the mT range. After fiber orientation, the fiber positions are interlocked by crosslinking the hydrogel precursor solution around the fibers, resulting in a stable Anisogel after removal of the magnetic field. Due to the low concentration of iron, this hybrid hydrogel concept is suitable for in vivo applications. The simplicity and versatility of this approach enables the formation of unidirectional, oriented structures in situ with controlled features that stimulate fibroblasts and functional nerve cells to grow in a linear manner. Importantly, the Anisogel supports unipolar neural signal propagation in direction of the oriented fibers, which is a crucial function for applications in linearly oriented neuronal tissues, such as spinal cord. This Anisogel opens the field for a new type of regenerative biomaterial that bridges the gap between implantable guiding scaffolds and low invasive isotropic injectable hydrogels. It provides a platform that can be applied as therapeutic material to heal different types of tissues that consist of an aligned architecture inside the body, such as the heart, kidney, muscles, and nerves. The elegant, high-throughput fiber fabrication method and low invasiveness of this technology can enhance the clinical outcome for patients without risking further damage and enable investigating the effect of an anisotropic matrix on physiological and pathological processes in vitro and in vivo.

Experimental Section

Experimental details can be found in the Supporting Information.

Supporting Information

Supporting Information is available from the Wiley Online Library or from the author.

Conflict of Interest

The authors declare no conflict of interest.

[1] a) M. Georgiou, S. C. J. Bunting, H. A. Davies, A. J. Loughlin, J. P. Golding, J. B. Phillips, *Biomaterials* **2013**, *34*, 7335; b) E. S. Place, N. D. Evans, M. M. Stevens, *Nat. Mater.* **2009**, *8*, 457; c) S. Jana, S. K. Levengood, M. Zhang, *Adv. Mater.* **2016**, *28*, 10588; d) D. Seliktar, *Science* **2012**, *336*, 1124.

[2] a) E. S. Place, N. D. Evans, M. M. Stevens, *Nat. Mater.* **2009**, *8*, 457; b) N. C. Rivron, J. Rouwkema, R. Truckenmuller, M. Karperien, J. De Boer, C. A. Van Blitterswijk, *Biomaterials* **2009**, *30*, 4851.

[3] S. Tawfick, M. De Volder, D. Copic, S. J. Park, C. R. Oliver, E. S. Polsen, M. J. Roberts, A. J. Hart, *Adv. Mater.* **2012**, *24*, 1628.

[4] a) J. Torbet, M. C. Ronzière, *Biochem. J.* **1984**, *219*, 1057; b) J. Torbet, J. M. Freyssinet, G. Hudry-Clergeon, *Nature* **1981**, *289*, 91; c) N. Dubey, P. C. Letourneau, R. T. Tranquillo, *Biomaterials* **2001**, *22*, 1065; d) D. Ceballos, X. Navarro, N. Dubey, G. Wendelschafer-Crabb, W. R. Kennedy, R. T. Tranquillo, *Exp. Neurol.* **1999**, *158*, 290.

[5] a) D. von Heimburg, S. Zachariah, I. Heschel, H. Kuhling, H. Schoof, B. Hafemann, N. Pallua, *Biomaterials* **2001**, *22*, 429; b) S. Stokols, M. H. Tuszynski, *Biomaterials* **2006**, *27*, 443; c) M. Chen, J. Zhu, G. Qi, C. He, H. Wang, *Mater. Lett.* **2012**, *89*, 104.

[6] a) K. Pawar, B. J. Cummings, A. Thomas, L. D. Shea, A. Levine, S. Pfaff, A. J. Anderson, *Biomaterials* **2015**, *65*, 1; b) L. De Laporte, A. des Rieux, H. M. Tuinstra, M. L. Zelivyanskaya, N. M. De Clerck, A. A. Postnov, V. Preat, L. D. Shea, *J. Biomed. Mater. Res., Part A* **2011**, *98*, 372.

[7] L. D. Laporte, Y. Yang, M. L. Zelivyanskaya, B. J. Cummings, A. J. Anderson, L. D. Shea, *Mol. Ther.* **2009**, *17*, 318.

[8] a) A. Kriebel, M. Rumman, M. Scheld, D. Hodde, G. Brook, J. Mey, *J. Biomed. Mater. Res., Part B* **2014**, *102*, 356; b) D. Hodde, J. Gerardo-Nava, V. Wohlk, S. Weinandy, S. Jockenhovel, A. Kriebel, H. Altinova, H. W. Steinbusch, M. Moller, J. Weis, J. Mey, G. A. Brook, *Eur. J. Neurosci.* **2016**, *43*, 376; c) E. Schnell, K. Klinkhammer, S. Balzer, G. Brook, D. Klee, P. Dalton, J. Mey, *Biomaterials* **2007**, *28*, 3012.

[9] N. Brandenberg, M. P. Lutolf, *Adv. Mater.* **2016**, *28*, 7450.

[10] M. A. Haque, G. Kamita, T. Kurokawa, K. Tsujii, J. P. Gong, *Adv. Mater.* **2010**, *22*, 5110.

[11] J. M. Corey, D. Y. Lin, K. B. Mycek, Q. Chen, S. Samuel, E. L. Feldman, D. C. Martin, *J. Biomed. Mater. Res., Part A* **2007**, *83*, 636.

[12] a) Y. Mu, F. Wu, Y. Lu, L. Wei, W. Yuan, *Nanomedicine* **2014**, *9*, 1869; b) H. Cao, T. Liu, S. Y. Chew, J. Xie, M. R. MacEwan, A. G. Schwartz, Y. Xia, *Adv. Drug Delivery Rev.* **2009**, *61*, 1055; c) Y. Yang, L. D. Laporte, M. L. Zelivyanskaya, K. J. Whittlesey, A. J. Anderson, B. J. Cummings, L. D. Shea, *Tissue Eng., Part A* **2009**, *15*, 3283.

[13] L. H. Nguyen, M. Gao, J. Lin, W. Wu, J. Wang, S. Y. Chew, *Sci. Rep.* **2017**, *7*, 42212.

[14] Z. Zhang, S. Yao, S. Xie, X. Wang, F. Chang, J. Luo, J. Wang, J. Fu, *Sci. Rep.* **2017**, *7*, 40017.

[15] D. Li, Y. Wang, Y. Xia, *Adv. Mater.* **2004**, *16*, 361.

[16] a) N. Amiraliyan, M. Nouri, M. H. Kish, *J. Appl. Polym. Sci.* **2009**, *113*, 226; b) T. Uyar, F. Besenbacher, *Polymer* **2008**, *49*, 5336; c) M. Mehrasa, A. O. Anarkoli, M. Rafienia, N. Ghasemi, N. Davary, S. Bonakdar, M. Naeimi, M. Agheb, M. R. Salamat, *Int. J. Polym. Mater. Polym. Biomater.* **2016**, *65*, 457.

[17] A. Sivashanmugam, R. Arun Kumar, M. Vishnu Priya, S. V. Nair, R. Jayakumar, *Eur. Polym. J.* **2015**, *72*, 543.

[18] D. Macaya, M. Spector, *Biomed. Mater.* **2012**, *7*, 012001.

[19] R. Ravichandran, J. R. Venugopal, S. Sundarrajan, S. Mukherjee, R. Sridhar, S. Ramakrishna, *Nanotechnology* **2012**, *23*, 385102.

[20] a) O. Regev, C. S. Reddy, N. Nseir, E. Zussman, *Macromol. Mater. Eng.* **2013**, *298*, 283; b) S. Poveda-Reyes, L. R. Mellera-Oglialoro, R. Martínez-Haya, T. C. Gamboa-Martínez, J. L. Gómez Ribelles, G. Gallego Ferrer, *Macromol. Mater. Eng.* **2015**, *300*, 977.

[21] M. Sawawi, T. Y. Wang, D. R. Nisbet, G. P. Simon, *Polymer* **2013**, *54*, 4237.

[22] K. Z. Chiaki Yoshikawa, E. Zawadzak, H. Kobayashi, *Sci. Technol. Adv. Mater.* **2011**, *12*, 7.

[23] T. G. Kim, T. G. Park, *Macromol. Rapid Commun.* **2008**, *29*, 1231.

[24] A. Stoiljkovic, S. Agarwal, *Macromol. Mater. Eng.* **2008**, *293*, 895.

[25] K. J. Lee, J. Yoon, S. Rahmani, S. Hwang, S. Bhaskar, S. Mitragotri, J. Lahann, *Proc. Natl. Acad. Sci. USA* **2012**, *109*, 16057.

[26] E. J. Berns, S. Sur, L. Pan, J. E. Goldberger, S. Suresh, S. Zhang, J. A. Kessler, S. I. Stupp, *Biomaterials* **2014**, *35*, 185.

[27] S. Zhang, M. A. Greenfield, A. Mata, L. C. Palmer, R. Bitton, J. R. Mantei, C. Aparicio, M. O. de la Cruz, S. I. Stupp, *Nat. Mater.* **2010**, *9*, 594.

[28] J. Kim, J. R. Staunton, K. Tanner, *Adv. Mater.* **2016**, *28*, 132.

[29] M. Antman-Passig, O. Shefi, *Nano Lett.* **2016**, *16*, 2567.

[30] T. R. Pisanic, J. D. Blackwell, V. I. Shubayev, R. R. Finones, S. Jin, *Biomaterials* **2007**, *28*, 2572.

[31] a) R. M. Erb, R. Libanori, N. Rothfuchs, A. R. Studart, *Science* **2012**, *335*, 199; b) M. B. Olaf Kriha, M. Lehmann, D. Kriha, J. Krieglstein, M. Yosef, S. Schlecht, R. B. Wehrspohn, J. H. Wendorff, A. Greiner, *Adv. Mater.* **2007**, *19*, 3; c) J. Liu, J. Shi, L. Jiang, F. Zhang, L. Wang, S. Yamamoto, M. Takano, M. Chang, H. Zhang, Y. Chen, *Appl. Surf. Sci.* **2012**, *258*, 7530.

[32] J. C. Rose, M. Camara Torres, K. Rahimi, J. Köhler, M. Moeller, L. De Laporte, *Nano Lett.* **2017**, *17*, 3782.

[33] A. Pal, A. Singh, T. C. Nag, P. Chattopadhyay, R. Mathur, S. Jain, *Int. J. Nanomed.* **2013**, *8*, 2259.

[34] a) X. Zong, S. Ran, K.-S. Kim, D. Fang, B. S. Hsiao, B. Chu, *Biomacromolecules* **2003**, *4*, 416; b) B. Duan, X. Yuan, Y. Zhu, Y. Zhang, X. Li, Y. Zhang, K. Yao, *Eur. Polym. J.* **2006**, *42*, 2013.

[35] S. M. Willerth, K. J. Arendas, D. I. Gottlieb, S. E. Sakiyama-Elbert, *Biomaterials* **2006**, *27*, 5990.

[36] a) K. J. Le Goff, C. Gaillard, W. Helbert, C. Garnier, T. Aubry, *Carbohydr. Polym.* **2015**, *116*, 117; b) X. Yang, E. Bakaic, T. Hoare, E. D. Cranston, *Biomacromolecules* **2013**, *14*, 4447; c) M. Baniasadi, M. Minary-Jolandan, *Materials* **2015**, *8*, 799.

[37] M. Ivenshitz, M. Segal, *J. Neurophysiol.* **2010**, *104*, 1052.

NANO | MICRO

small

Supporting Information

An Injectable Hybrid Hydrogel with Oriented Short Fibers Induces Unidirectional Growth of Functional Nerve Cells

Abdolrahman Omidinia-Anarkoli, Sarah Boesveld, Urandelger Tuvshindorj, Jonas C. Rose, Tamás Haraszti, and Laura De Laporte*

Supporting Information

An injectable hybrid hydrogel with oriented short fibers induces unidirectional growth of functional nerve cells

Abdolrahman Omidinia-Anarkoli, Sarah Boesveld, Urandelger Tuvshindorj, Jonas C. Rose, Tamás Haraszti, Laura De Laporte *

SPION synthesis: SPIONs are prepared as previously described.[1] Briefly, 2.3 g ammonium iron (II) sulfate hexahydrate $(NH_4)_2Fe(SO_4)_2$ $6H_2O$ (Sigma-Aldrich, Germany) is dissolved in 10 mL distilled water in a 100 mL three-necked flask under nitrogen, followed by the addition of 10 mL oleic acid vegetable (VWR, Germany), 10 mL 25 % (w/w) tetramethylammonium hydroxide solution $(CH_3)_4N(OH)$ (Sigma-Aldrich, Germany), and 35 mL DMSO (Sigma-Aldrich, Germany). The mixture is mixed with a glass stirrer and refluxed at 140 °C for 1 h. Superparamagnetic iron oxide nanoparticle (SPION) precipitates are obtained and washed with excess of ethanol by magnetic separation (Figure S1a).

Short fiber fabrication via electrospinning/cryosectioning: Poly(lactide-co-glycolide) (PLGA) (75:25, RESOMER® RG 756 S, Evonik Industries) is dissolved in 90:10 v/v chloroform: DMF (Sigma–Aldrich, Germany) at a concentration of 18 w/v%. Different amounts of synthesized SPIONs (1, 5 and 10 of polymer w/w%) are dispersed into the polymer solution using 10 min of ultrasonication (Sonifier W-250D Brandson) prior to the electrospinning process. The distribution of 10 w/w% SPIONs to PLGA in solution is analyzed by pipetting 5 µL of the solution on a standard carbon-coated transmission electron microscopy (TEM) grid at two

different time points: immediately after the ultrasonication step and 1 hour after sonication, which is the time it takes to spin the fibers. The SPIONs inside the thin layer of dried PLGA solution are visualized using scanning transmission electron microscopy (STEM) (HITACHI, SU9000) (Figure S1b and S1c). The polymer solution, mixed with or without SPIONs, is electrospun with a fixed flow rate of 0.5 mLh^{-1}, while the voltage is varied in the range of 7–8.5kV. A parallel plate collector (2 cm gap) is used to collect fibers in an aligned manner, as previously described (Figure S2a).[2] The SPION distribution inside the PLGA fibers is analyzed after electrospinning by visualizing fiber cross-sections with TEM (Zeiss, Libra 120). Fibers are embedded in an epoxy (EpoFix-Satz) and incubated at 35°C over night. Using a 45° diamond knife (PowerTome Ultramicrotome XL), 70 nm thickness sections are harvested directly on a TEM grid and sequentially visualized (Figure S1d).

In order to render the fibers fluorescent, two methods of modification are applied. In the first one, 18 w/v% PLGA solution is mixed with NCO-sP(EO-stat-PO), covalently bound to Fluoresceinamine, isomer I, and electrospun using a previously reported method to render PLGA fibers with a fluorescent PEG coating.[3] To enable mixing of the fibers with cells, Rhodamin B (Sigma-Aldrich, Germany) is mixed with the polymer solution at a fixed concentration of 0.1 w/w% of the polymer, representing the second method.

Short fibers are prepared as previously described.[4] Briefly, aligned nanofibers are harvested from the parallel plate collector and placed in a custom designed polyethylene cryomold. Optimal cutting temperature (OCT) gel (Sakura Finetec) is added and the aligned fibers are frozen inside the mold by immersion in liquid nitrogen. The resulting block of solidified gel with aligned fiber stack embedded therein is sectioned perpendicular to the direction of fibers, using a cryostat microtome (Leica CM3000 Cryosat) maintained at -20°C. Harvested sections are

allowed to warm up to room temperature, followed by dissolution of the OCT gel and repeating washing steps with distilled water (Figure S2b-d).

Fiber Characterization: Electron microscopy of fibers is done via field emission scanning electron microscopy (HITACHI S-4800) of gold sputtered (using physical vapor deposition) fibers. Here, fibers without SPIONs and with 1, 5, and 10 w/w% SPIONs are analyzed (Figure S3a). The diameter and length distribution of the short fibers are manually quantified by analyzing 80-100 randomly selected long and short fibers, respectively, using Image J.

Quantification of iron content: Thermal analysis of the SPION solution, PLGA fibers without SPIONs, and PLGA fibers with 10 w/w% SPIONs is performed by thermogravimetric analysis (TGA). The organic phases (oleic acid coating, PLGA) are burnt under a nitrogen atmosphere at a heating rate of 10 °C/min from room temperature up to 1000 °C, followed by complete burning at 1000 °C for 30 min. The residual weight after burning is used to calculate the iron content of the SPIONs, and subsequently the SPION encapsulation efficiency inside the fibers during preparation (Figure S3b).The first mass loss occurs around 210°C, most likely marking the removal of ethanol adsorbed on the particle surface and free oleic acid.[5] The largest step in weight loss occurs around 300 °C and is mainly attributed to the decomposition and subsequent evaporation of the coating layer.[6] For the synthesized SPION solution, the TGA residual mass is 31.0 ± 0.6 % of the total dried SPION solution, which is likely to be the remaining inorganic iron content of the SPIONs. The TGA curve of PLGA fibers without SPIONs demonstrate complete degradation of fibers at around 500°C, similar to previous reports.[7] Based on the calculated 31 % iron present in the SPIONs, fibers fabricated with 10 w/w% SPIONs could contain maximum 3.1 ± 0.1 w/w% iron (Figure S3c). TGA measurements of fibers fabricated with 10 w/w% SPIONs, therefore, reveal a SPION encapsulation efficiency of 78 %. The 22 % loss in

iron encapsulation may be due to sample preparation, the ultrasonication step, and the electrospinning process.

Rheological behavior of hydrogels: The mechanical properties of hydrogels with and without short fibers are evaluated by a Discovery Hybrid Rheometer (TA Instruments HR-3 Rheometer PHR3, Waters, Milford, USA), equipped with a conical geometry with 20 mm diameter and a heating plate (2˚ inclination, waters, Milford, USA) (Figure S4). All experiments are performed at a constant temperature of 37 °C and in order to prevent hydrogel dehydration during the measurement time, a solvent trap is used. The storage and loss moduli of the hydrogels without fibers and with randomly oriented and aligned fibers are obtained in a time sweep experiment using a frequency of 0.5 Hz and strain of 0.5%. Hybrid hydrogel solutions are prepared and carefully pipetted in the center of the device's bottom plate. In order to obtain the correct hydrogel geometry and good contact with the probe, the probe is lowered 3 min after pipetting the hydrogel to start the measurements (n=3). In the case of Anisogels, a home-made magnetic insert (5 cm gap, 100 mT) is used to orient the fibers parallel to the bottom plate before lowering the probe.

Analysis of the fiber orientation time inside an external magnetic field: The orientation time of the short magneto-responsive fibers is determined by analyzing the fiber dispersion on a standard microscope slide placed on an optical microscope (Zeiss, Axio Observer, Z1). Standard cuvette magnets (LUMiSizer) with magnetic field strengths of 100, 200, and 300 mT are placed on the glass slide, while 20 μL of the fiber dispersion is pipetted exactly in the center of the 1 cm gap between the magnets. The time-lapse images (every 1-10 seconds, depending on SPION concentration and fiber length) of the fibers are imported in ImageJ and analyzed using the plugin OrientationJ. The dominant orientation and the coherency (relative to maximum

coherency) of figures are measured (n=5) and the time, at which the relative coherency changes less than 0.1 % per second over an interval of 5 s, is determined to be the orientation time.

DRG dissection and dissociation: DRGs are isolated from E9-10 chick embryos as previously reported.[8] DRGs are harvested from both sides of the spinal column and after removal of the excess tissue, stored in HBSS (Hank's buffered saline solution, Life Technologies) for up to 3 h, prior to placement in hydrogels or the required dissociation step to obtain single neurons. For dissociation, DRGs are incubated for 30 minutes at 37 ºC in 10X trypsin (Sigma-Aldrich, Germany), followed by trituration with fire-polished glass Pasteur pipettes to dissociate the ganglia. Neuronal cells are separated by panning for maximum 2 hours at 37 ºC.[9]

Cell culture inside hybrid hydrogels: Fibrin gels, containing fibrinogen (8 mg/ml in the case of fibroblasts and 4 mg/ml for DRGs and nerve cells) and an activated enzyme solution, consisting of factor XIII (fibrogrammin, 4 U/mL), thrombin (0.25 U/mL), and calcium chloride (5 mM) in HEPES buffer, are prepared with and without magnetic fibers containing 10 w/w% SPIONs, in the absence and presence of an external magnetic field. In the case of L929 mouse fibroblasts or primary neurons, a cell suspension of 500,000 cell/mL gel or 5,000,000 cell/mL gel, respectively, is directly mixed within the hydrogel solution and injected in a single glass-bottom PDMS well. In the case of full DRGs, the DRGs are inserted inside the gel during gelation. To obtain fiber alignment, the cell loaded gels are placed inside a magnetic insert (100 mT). After crosslinking of the hydrogels, the PDMS wells are transferred to a 24 well plate with 1.5 mL basal medium, comprising RPMI, supplemented with 10 % fetal bovine serum and 1 % antibiotics/antimycotics, supplied by Gibco Thermo Fisher Scientific (for fibroblast samples) or 1.5 mL of DMEM, supplemented with 10 % fetal bovine serum, 1 % antibiotics/antimycotics, 20 ng/mL NGF and 8 µg/ml Aprotinin (in the case of primary neurons and DRG samples).

Fibroblasts are cultivated for 2 days at 37 °C, 5 % CO2 and 95 % humidity, whereas primary neurons and DRGs are incubated at the same conditions for 7 days. Aprotinin from bovine lung is added at a fixed concentration of 8 µg/mL gel to the media for hydrogels containing DRGs or primary neurons to slow down the degradation of fibrin gel during the 7 days of culture.

Immunostaining: The immunostaining is performed as previously described.[10] Briefly, samples are fixed with 4 % paraformaldehyde, permeabilized with 0.1 % Triton X-100, and blocked with 2 % bovine serum albumin (BSA) in PBS. Fibroblast actin is stained by Alexa Fluor 594 Phalloidin (1:100) and the nucleus is stained with 4',6-diamidino-2-phenylindole (DAPI) at the concentration of 2 % (v/v) in PBS. Neurons are stained with a neurotubulin antibody (1:250 TUJ1 monoclonal antibody mouse-derived), followed by a secondary fluorescent antibody (1:100 Rhodamine (TRITC) goat-derived anti-mouse antibody). Images of the immuno-stained fibroblasts, primary neurons, and DRGs inside the 3D hybrid hydrogels are acquired using Laser scanning confocal microscopy (Leica) with a 20X oil or 10X objective.

Image analysis: A program based on Python code is applied to analyze the orientation of the short fibers, fibroblasts, and neurites inside the hydrogels.[11] Briefly, all the images are smoothened with a Gaussian filter (standard deviation of 0.75 pixels) after background correction using a rolling ball filter. Following image smoothening, an asymmetric Mexican hat filter (a Laplace operator applied to a 2-dimensional Gaussian function) with standard deviations of 10 pixels in x-direction and 1.0 pixels in y-direction, rotated to 20 angle values between − 90 and 90 degrees, is applied to the images. The maximum of each pixel along the various angles is recorded (maximum image) (Figure S5), as well as the angle where this maximum is found (angle image). The maximum image is then filtered using an automatic threshold (Otsu's method) and only values above this threshold are kept. The obtained angle values are converted

to a histogram, which is rotated such that the maximum is directed to 0 degrees. Full width at half maximum (FWHM) of the angular distributions is calculated to quantitatively compare the orientation of each group (Figure S6). For each hydrogel type (comprising aligned, random or no fiber), three DRGs are quantified, and using an ImageJ plugin, NeuronJ, ten distinct neurite lengths are measured based on previous published reports.[12] The length of the neurites is measured via tracing from their origin at the perimeter of the ganglion until its end, considering changes in direction along its course.

Calcium imaging: Gels (30 µL) are seeded with 30,000 neurons and injected into Ibidi µ-slides (8 well) in the presence or absence of a magnetic field. The cells are cultured for 7 days, after which they are washed with HBSS supplemented with glucose (1 g/L). Calcium imaging reagent solution is added, including HBSS with glucose, Fluo-4-AM, loading buffer, and probenecid, to measure spontaneous neuronal electrochemical activity in accordance to the Fluo-4 Calcium imaging kit by Molecular Probes. After 45 min incubation, samples are washed with HBSS once and then imaged in HBSS with a confocal laser scanning microscope (Leica SP8 Tandem Confocal system, equipped with a white light laser (WLL) and a cultivation chamber heated to 37 °C). Samples are excited at 494 nm and detected via a photon counting HyD detector from 504 - 600 nm and a pinhole of ~ 2 Airy Unit with a scanning rate of 1000, achieving an acquisition rate of ~ 0.25 images/s. Imaging is conducted within the first 60 min. Regions of interest (3 x 3 µm) are determined and quantified via Leica Application Suite X. Normalization is conducted by determining the mean ground level fluorescence intensity F over a course of 10 frames, calculating the difference between each state F_n and F (defined as ΔF), and dividing $\Delta F/F$.

Statistical analysis: Statistical analysis is performed with OriginPro 2016G. A one-way ANOVA is executed with post-hoc Tukey comparison for evaluation of statistical significance between groups (*p < 0.05). Data are shown as mean average with error bars indicating the standard deviation.

References

[1]	C. Y. Wang, J. M. Hong, G. Chen, Y. Zhang, N. Gu, *Chin. Chem. Lett.* **2010**, *21*, 179.
[2]	a) R. Dersch, T. Liu, A. K. Schaper, A. Greiner, J. H. Wendorff, *J. Polym. Sci., Part A: Polym. Chem.* **2003**, *41*, 545; b) P. D. Dalton, D. Klee, M. Möller, *Polymer* **2005**, *46*, 611; c) D. Li, Y. Wang, Y. Xia, *Adv. Mater.* **2004**, *16*, 361.
[3]	D. Grafahrend, K.-H. Heffels, M. V. Beer, P. Gasteier, M. Möller, G. Boehm, P. D. Dalton, J. Groll, *Nat. Mater.* **2011**, *10*, 67.
[4]	K. J. Lee, J. Yoon, S. Rahmani, S. Hwang, S. Bhaskar, S. Mitragotri, J. Lahann, *PNAS* **2012**, *109*, 16057.
[5]	a) F. Ozel, H. Kockar, S. Beyaz, O. Karaagac, T. Tanrisever, *J. Mater. Sci.: Mater. Electron.* **2013**, *24*, 3073; b) S. G. Kwon, Y. Piao, J. Park, S. Angappane, Y. Jo, N.-M. Hwang, J.-G. Park, T. Hyeon, *J. Am. Chem. Soc.* **2007**, *129*, 12571.
[6]	Shan, Zhi, Yang, Wan-Shen, Zhang, Xu, Huang, Qian-Ming, Ye, Hui, *J. Braz. Chem. Soc.* **2007**.
[7]	M. F. Silva, A. A. W. Hechenleitner, J. M. Irache, A. J. A. d. Oliveira, E. A. G. Pineda, *J. Mater. Sci.* **2015**, *18*, 1400.
[8]	A. M. Hopkins, L. De Laporte, F. Tortelli, E. Spedden, C. Staii, T. J. Atherton, J. A. Hubbell, D. L. Kaplan, *Adv. Funct. Mater.* **2013**, *23*, 5140.
[9]	L. De Laporte, A. Huang, M. M. Ducommun, M. L. Zelivyanska, M. O. Aviles, A. F. Adler, L. D. Shea, *Acta Biomater.* **2010**, *6*, 2889.
[10]	J. C. Rose, M. Camara Torres, K. Rahimi, J. Köhler, M. Moeller, L. De Laporte, *Nano Lett.* **2017**, *17*, 3782.
[11]	D. Missirlis, T. Haraszti, C. v. C. Scheele, T. Wiegand, C. Diaz, S. Neubauer, F. Rechenmacher, H. Kessler, J. P. Spatz, *Sci. Rep.* **2016**, *6*, 23258.
[12]	a) M. T. Abu-Rub, K. L. Billiar, M. H. van Es, A. Knight, B. J. Rodriguez, D. I. Zeugolis, S. McMahon, A. J. Windebank, A. Pandit, *Soft Matter* **2011**, *7*, 2770; b) J. M. Corey, D. Y. Lin, K. B. Mycek, Q. Chen, S. Samuel, E. L. Feldman, D. C. Martin, *J. Biomed. Mater. Res., Part A* **2007**, *83*, 636.
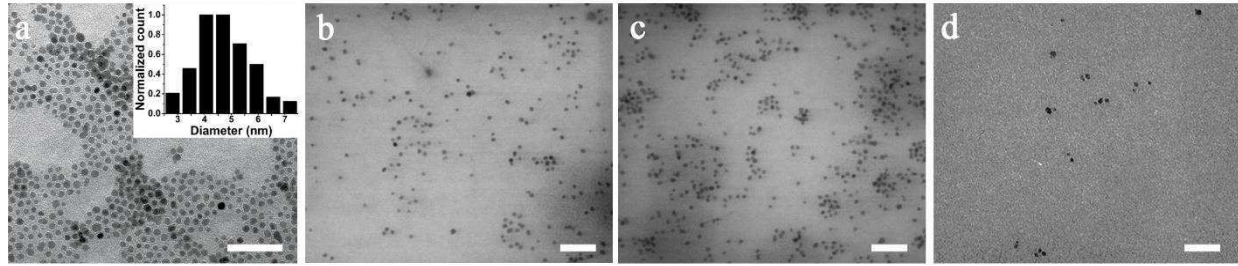
Figure S1: (a) TEM image of synthesized SPIONs with an average diameter of 5.2 ± 1.0 nm (inset image). (b-c) Homogenous SPION distribution in a thin layer of dried PLGA solution directly after ultrasonication (b) and 1h after the ultrasonication step, which is the time it takes to spin the fibers. (d) Homogenous SPION distribution inside the electrospun fibers after sectioning. Scale bars 50 nm
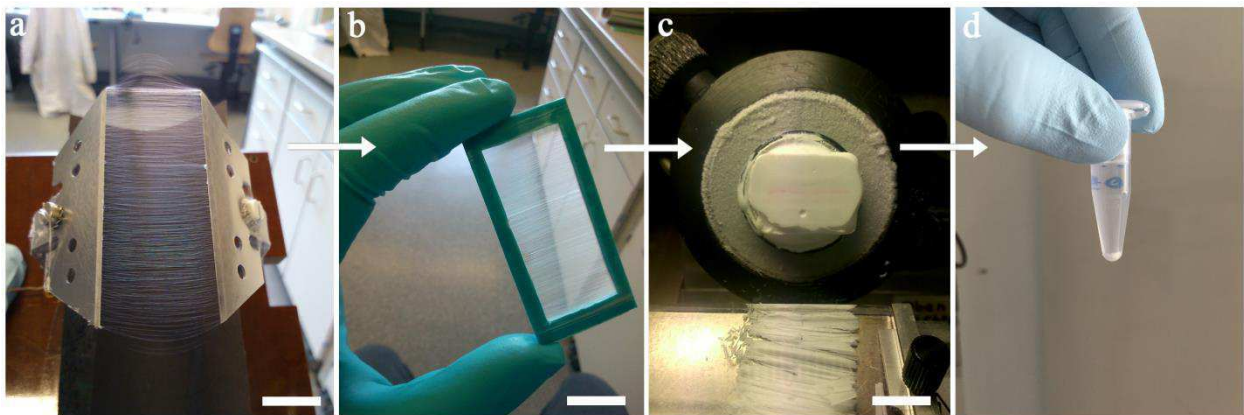

Figure S2: The experimental procedure of short fiber fabrication. (a) Aligned PLGA fibers collected on parallel plates. (b) Fibers are harvested from the collector with the help of a frame prior to freezing step. (c) Using a cryostat microtome device, the aligned fiber stack, embedded in a solidified frozen OCT gel, is sectioned perpendicular to the direction of fibers. (d) Harvested sections are allowed to warm up to room temperature, followed by dissolution of the OCT gel and repeating washing steps, to obtain the final suspension of short fibers in distilled water. Scale bars 1cm.
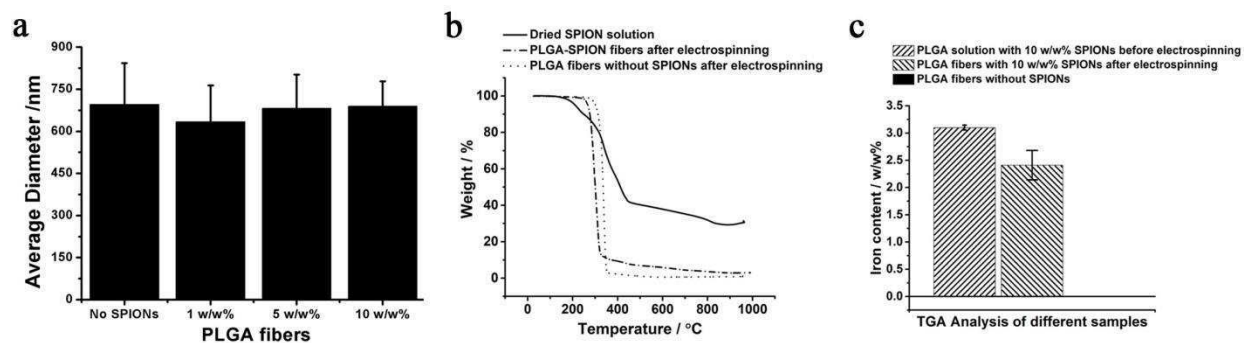
Figure S3: (a) The effect of SPION incorporation on the average diameter of the fibers. TGA analysis of SPION and electrospun fibers. (a) Results for dried SPION solution, and PLGA fibers without and with 10 w/w% SPIONs. (b) Iron content of a PLGA solution containing 10 w/w% SPIONs before electrospinning, and fibers containing SPION after electrospinning. Electrospun fibers without any SPIONs are shown as the baseline.
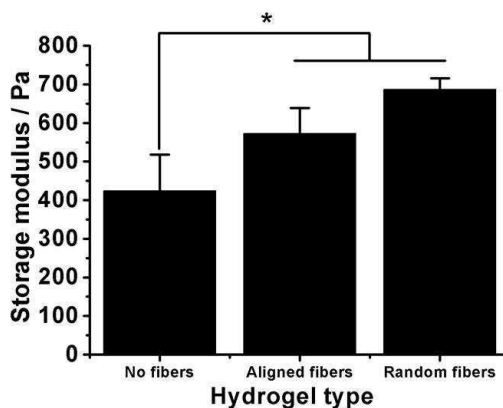

Figure S4: Storage moduli of fibrin gels (4 mg/mL) without fibers, and with random or aligned fibers.
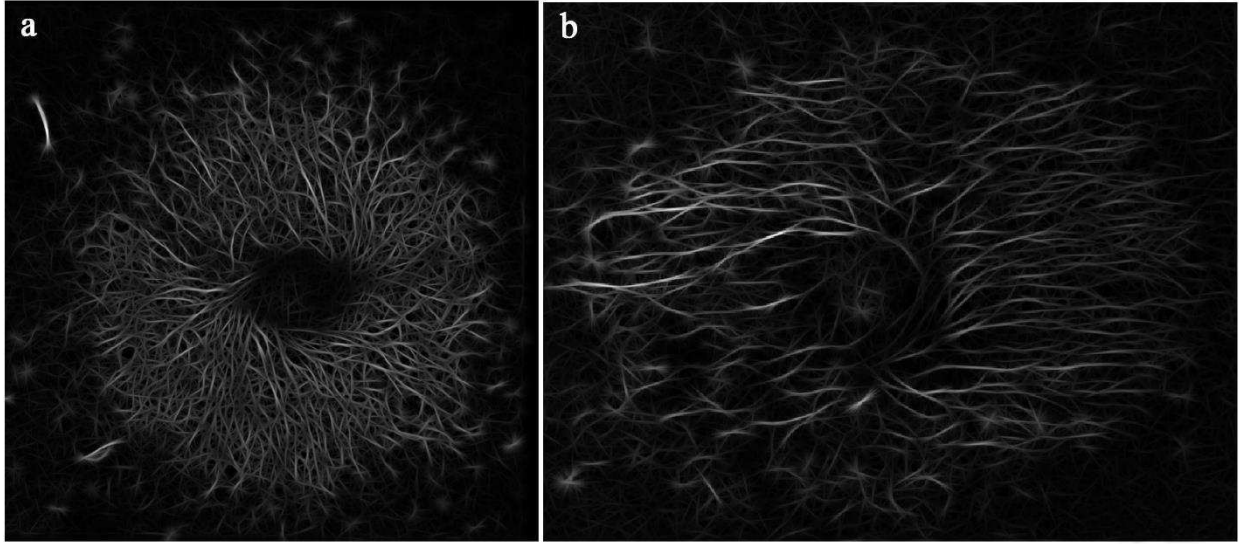
Figure S5: The maximum images of each pixel along the various angles recorded for a DRG cultured inside a fibrin gel with (a) randomly oriented fibers and (b) unidirectionally oriented fibers, corresponding to the Figure 3b and 3c, respectively.
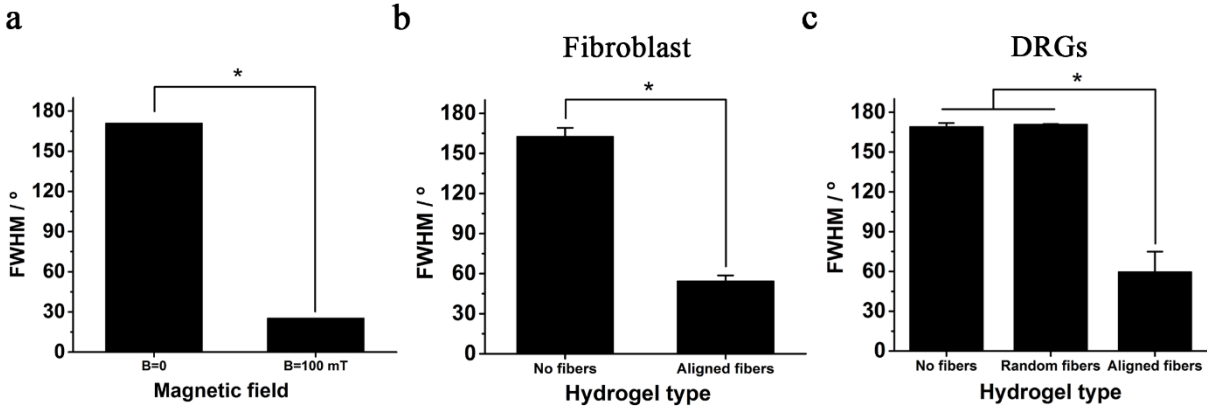

Figure S6: (a) FWHMs for the angular distributions of the short fibers in a hydrogel without or with an external magnetic field, corresponding to Figure 1g. (b) FWHMs of fibroblast elongation in hydrogels without fibers or aligned fibers, corresponding to Figure 2d. (c) FWHMs of DRG extensions in hydrogels without fibers, or with random or aligned fibers, corresponding to Figure 3g. *$p < 0.05$
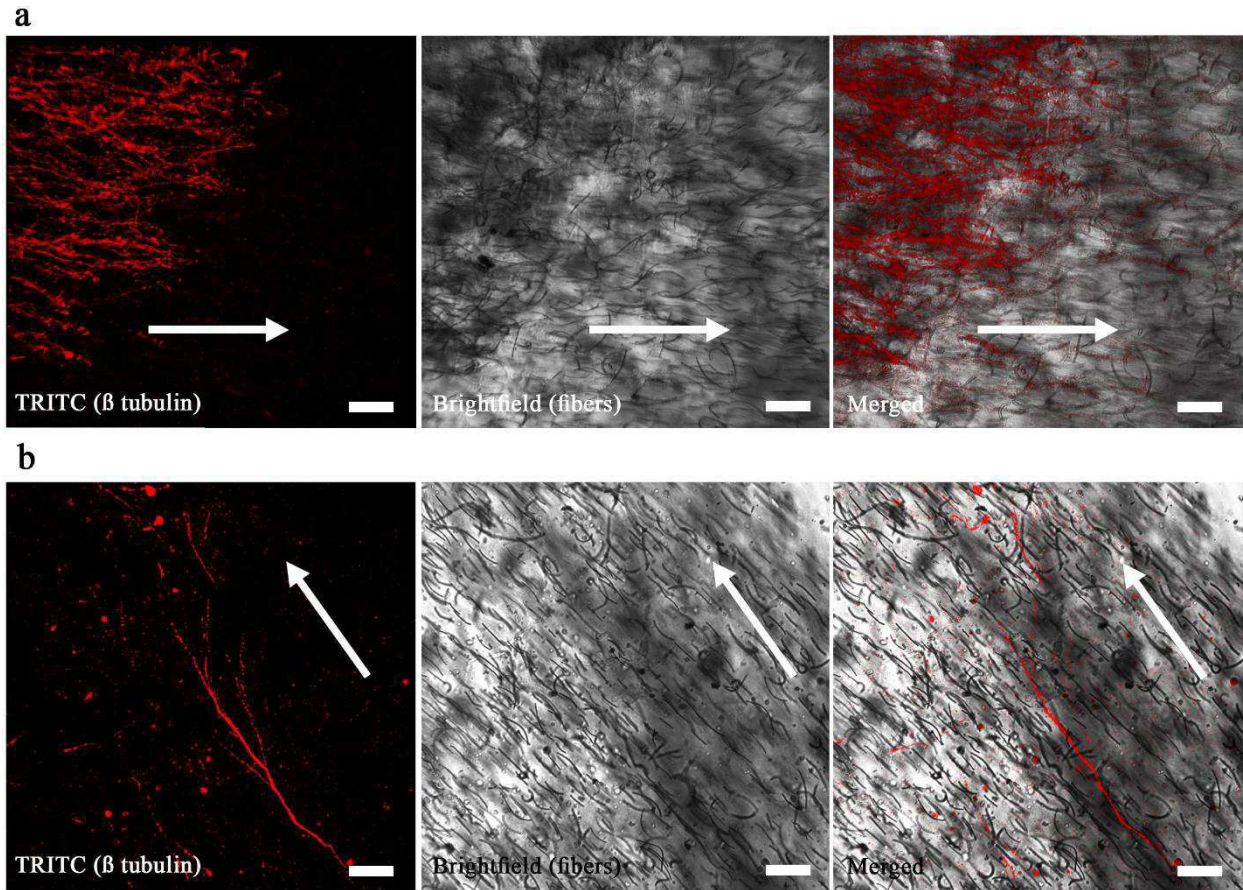
Figure S7: Anisogel functionality in nerve guidance. High magnification images of neurite extensions from a DRG explant (a) and a single neuron (b) (red: ß tubulin detected with TRITC) in the direction of the oriented fibers inside a 3D hydrogel network (bright field). Figure S6a corresponds to the white dashed box in Figure 3c. Scale bars 100 µm.
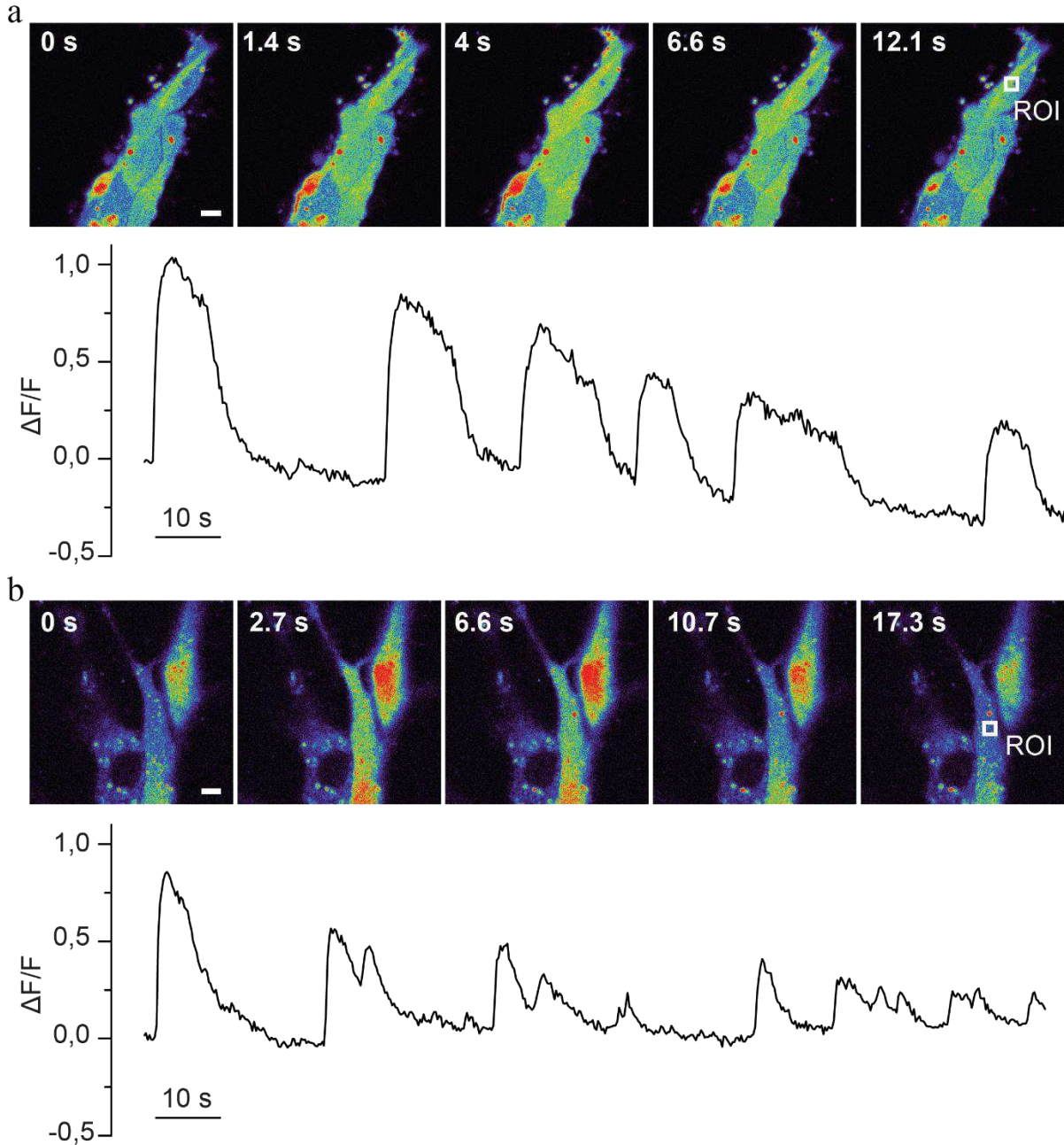
Figure S8: Normalized calcium signals inside neurons, grown inside the Anisogel. (a) Image sequence of the calcium transitions and signal quantification from Movie S3. (b) Image sequence of the calcium transitions and signal quantification from Movie S4. Signals are quantified from a region of interest with an area of 3 x 3 μm inside the cell body.

Movie S1: Magnetic orientation of short fibers with a length of 50 μm, doped with 5 w/w% SPIONs in an external magnetic field of 300 mT.

Movie S2: Calcium signals inside a neuron, grown inside the Anisogel. Image sequence of one calcium transition and the normalized quantification of calcium transitions in three different regions of the cell over a timespan of 14.6 s are displayed in Figure 4b. Movie is accelerated to 10 times real time.

Movie S3-S4: Calcium signals inside neurons inside the Anisogel. Image sequence of one calcium transition and the normalized quantification of calcium transitions over a timespan of 12.2 and 17.3 s, respectively, are displayed in Figure S8a and S8b. Movie is accelerated to 10 times real time.

Movie S5: Calcium signals along neurons inside a hydrogel with randomly oriented fibers. The signals propagate in multiple directions. Movie is accelerated to 10 times real time.

Movie S6: Calcium signals along neurons inside an Anisogel. Signal propagation occurs in the direction of the fiber alignment. Movie is accelerated to 10 times real time. Circles mark the regions of increasing calcium signals.